A long-term Global LAnd Surface Satellite (GLASS) data-set for environmental studies

Shunlin Liang, Xiang Zhao, Suhong Liu, Wenping Yuan, Xiao Cheng, Zhiqiang Xiao, Xiaotong Zhang, Qiang Liu, Jie Cheng, Hairong Tang, Yonghua Qu, Yancheng Bo, Ying Qu, Huazhong Ren, Kai Yu & John Townshend

Published online: 15 Jul 2013.

Submit your article to this journal

Article views: 5304

View related articles

Citing articles: 114 View citing articles

Taylor & Francis
Taylor & Francis Group

A long-term Global LAnd Surface Satellite (GLASS) data-set for environmental studies

Shunlin Liang[a,b,c]*, Xiang Zhao[a,b], Suhong Liu[a,d], Wenping Yuan[a,b], Xiao Cheng[a,b], Zhiqiang Xiao[a,d], Xiaotong Zhang[a,b], Qiang Liu[a,b], Jie Cheng[a,b], Hairong Tang[e], Yonghua Qu[a,b], Yancheng Bo[a,d], Ying Qu[a,d], Huazhong Ren[a,d], Kai Yu[e] and John Townshend[c]

[a]The State Key Laboratory of Remote Sensing Science, Jointly Sponsored by Beijing Normal University and Institute of Remote Sensing Applications of Chinese Academy of Sciences, Beijing, China; [b]College of Global Change and Earth System Sciences, Beijing Normal University, Beijing, China; [c]Department of Geographical Sciences, University of Maryland, MD, USA; [d]School of Geography, Beijing Normal University, Beijing, China; [e]Institute of Electronics, Chinese Academy of Sciences, Beijing, China

Recently, five Global LAnd Surface Satellite (GLASS) products have been released: leaf area index (LAI), shortwave broadband albedo, longwave broadband emissivity, incident short radiation, and photosynthetically active radiation (PAR). The first three products cover the years 1982–2012 (LAI) and 1981–2010 (albedo and emissivity) at 1–5 km and 8-day resolutions, and the last two radiation products span the period 2008–2010 at 5 km and 3-h resolutions. These products have been evaluated and validated, and the preliminary results indicate that they are of higher quality and accuracy than the existing products. In particular, the first three products have much longer time series, and are therefore highly suitable for various environmental studies. This paper outlines the algorithms, product characteristics, preliminary validation results, potential applications and some examples of initial analysis of these products.

Keywords: earth observation; global environmental change; remote sensing

1. Introduction

In order to advance global and regional land surface models at different scales and improve their predictive capabilities and other applicability to other uses, various space agencies have produced a series of high-level land surface biogeophysical products from different satellite data. Considerable progress has been made and different products have been used extensively for a variety of applications (Liang, Li, and Wang 2012). The quality, accuracy, and spatial-temporal coverage of these products, however, still require significant improvements.

There remain many issues in generating these products from satellite data, which have a direct impact on their quality and accuracy. Firstly, data from multiple highly complementary sensors have not been used effectively in generating the same high-level land products. Most satellite products have been generated from individual

---

sensors that usually cover the same short periods as the satellite missions. For example, leaf area index (LAI) products are produced from the Moderate Resolution Imaging Spectroradiometer (MODIS) and the Multi-angle Imaging SpectroRadiometer (MISR) sensors separately, although they are in the same satellite platform (Terra). Efforts are being made to produce the climate data record (CDR) from multiple satellite data-sets, defined by the National Research Council (NRC 2004) as a time series of measurements of sufficient length, consistency, and continuity to determine climate variability and change. However, most satellite land products still cover only short time series. Secondly, each product is generated primarily from one instrument algorithm, but as a rule it is almost impossible to identify the best algorithm as most of them perform optimally only under certain conditions. Thus, the accuracy of the specific product is not consistent under variable conditions. Finally, most instrument algorithms have not retrieved surface variables using multi-temporal signatures and most satellite inversion algorithms have not objectively incorporated a-priori knowledge. To improve the quality and accuracy of satellite products, efforts are needed to fully address these issues.

China has recently invested substantial resources to expand and improve on its Earth observation capabilities. Although some experimental high-level products have been generated, China has been unable to generate and distribute global land products. To achieve those goals, China launched the 863 key project entitled 'Generation and application of global products of essential land variables.' The central component of this project is the development of the Global LAnd Surface Satellite (GLASS) product production system, which generates five land products: LAI, shortwave broadband albedo, longwave broadband emissivity, downwelling shortwave radiation, and photosynthetically active radiation (PAR).

Key strategies of this project include the development of an integrated system that can produce multiple products from multiple satellite observations, exploring the use of multiple algorithms for the same product to improve accuracy and stability, and optimizing the use of temporal signatures in remote sensing data and the existing satellite high-level products.

These five products have been recently released to the public. To facilitate their extensive use, this paper aims to provide an overview of these products. In Section 2, we will briefly introduce the GLASS product generation system, including the execution of some preprocessing tasks. In Sections 3–7, individual products are described in detail, including a brief introduction to the needs of such a product, current satellite products and their limitations, GLASS product algorithms, and preliminary validation results.

2. Production system, preprocessing, and overall characteristics of GLASS products

Figure 1 shows a schematic diagram of the hardware devices and inter-connectivities within the GLASS products production system. The hardware primarily comprises a data processing server and a production management server. The data processing server is either a high-performance computer or a PC cluster. The production management server comprises a task management server, a resource monitoring server, a production-scheduling server, and a quality inspection server. The data management system hardware mainly comprises a database management server, a
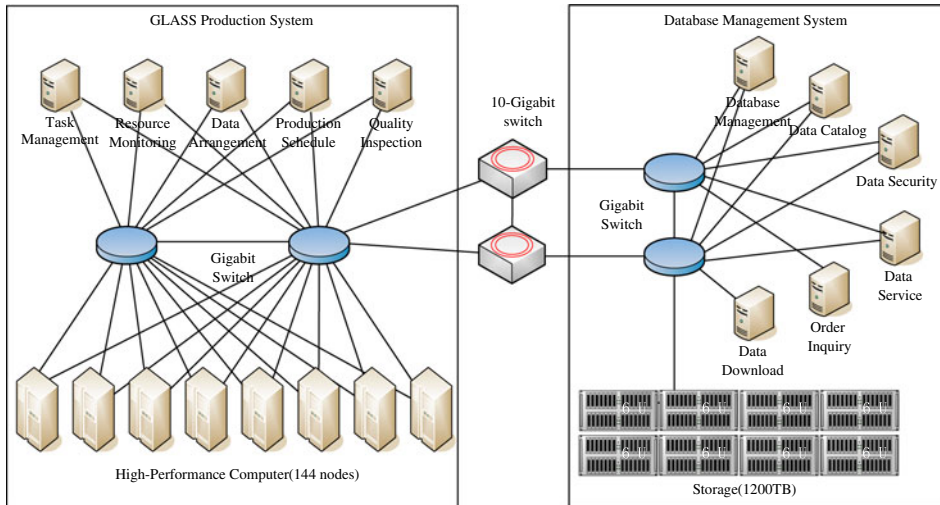
Figure 1. Hardware configuration for the GLASS product production system.

mass data storage system, and a product distribution server, all of which are interconnected via a 10 GB switch or 1 GB switch.

The hardware-specific parameters of the GLASS production system are listed in Table 1, and comprise a computation server, a storage system, a database management server, a distribution server, a switch, and other devices.

A series of preprocessing tasks have been executed to produce improved algorithm inputs to allow the generation of the high-level products. The first group of techniques is used mainly to process the MODIS surface reflectance product. To detect and remove remaining cloudy or partially cloudy pixels in the MODIS surface

Table 1. Specifics of the hardware devices within the GLASS product production system.

| Number	Name	Major equipment parameters
1	Computation server	One hundred and forty four computation nodes with a double quad-core CPU for each node; 1 GB/10 GB switch
2	Production management server	Five classes of system management servers: task management, resource monitoring, data arrangement, production scheduling, and quality inspection
3	Storage system	SAS storage: capacity 200 TB;15 krpmSAS hard disk; IOPS no less than 650 thousand; and 2 RAID cards for each IO node, totaling 24 SATA storage: capacity 500 TB; SATA 7200 rpm hard drive; IOPS no less than 650 thousand; 2 RAID cards for each IO node, totaling 24 Mobile disk: capacity 500 TB; SATA 7200 rpm hard drive, mainly used for data download and back-up
4	Database management server	Six classes database management servers: database management, data catalog, data security, data service, order inquiry, and data download
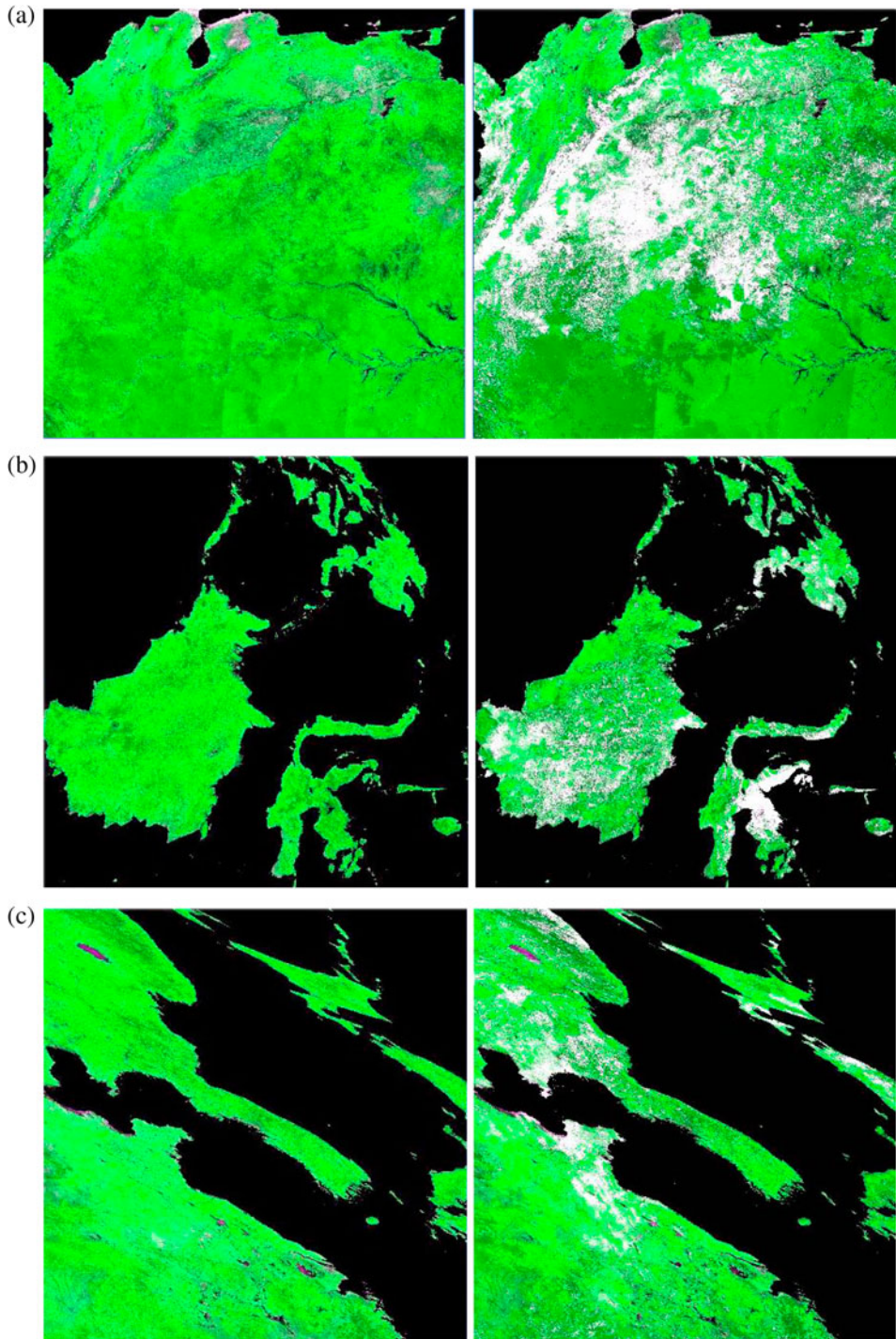
Figure 2. Three examples of the improved MODIS surface reflectance images using the TSCD algorithm (left) compared to the original MOD09A1 (right): (a) Amazon, (b) Java, Indonesia, (c) Bohai area of eastern Asia. All images were acquired on 28 July 2001.

reflectance product (MOD09A1), a new time series cloud detection (TSCD) algorithm is implemented (Tang et al. 2012). TSCD is based on the assumption of relatively stable surface reflectance and of rapid temporal variations in reflectance due to cloud contamination. The validation results demonstrated that the TSCD algorithm performs very well, particularly when the land surface is stable or changing slowly. A temporal spatial filter method that integrates temporal, spatial, spectral, and flag information has also been executed to better separate cloudy and snow pixels and to fill any gaps. Some examples are shown in Figure 2.

These spatio-temporal filtering techniques have been extended to improve Advanced Very High Resolution Radiometer (AVHRR) data; one example is shown in Figure 3.

Five GLASS products have been generated and were released to the public in November 2012. To facilitate and promote the utilization of these five products, the user requirements for each product, the retrieval algorithms, and preliminary
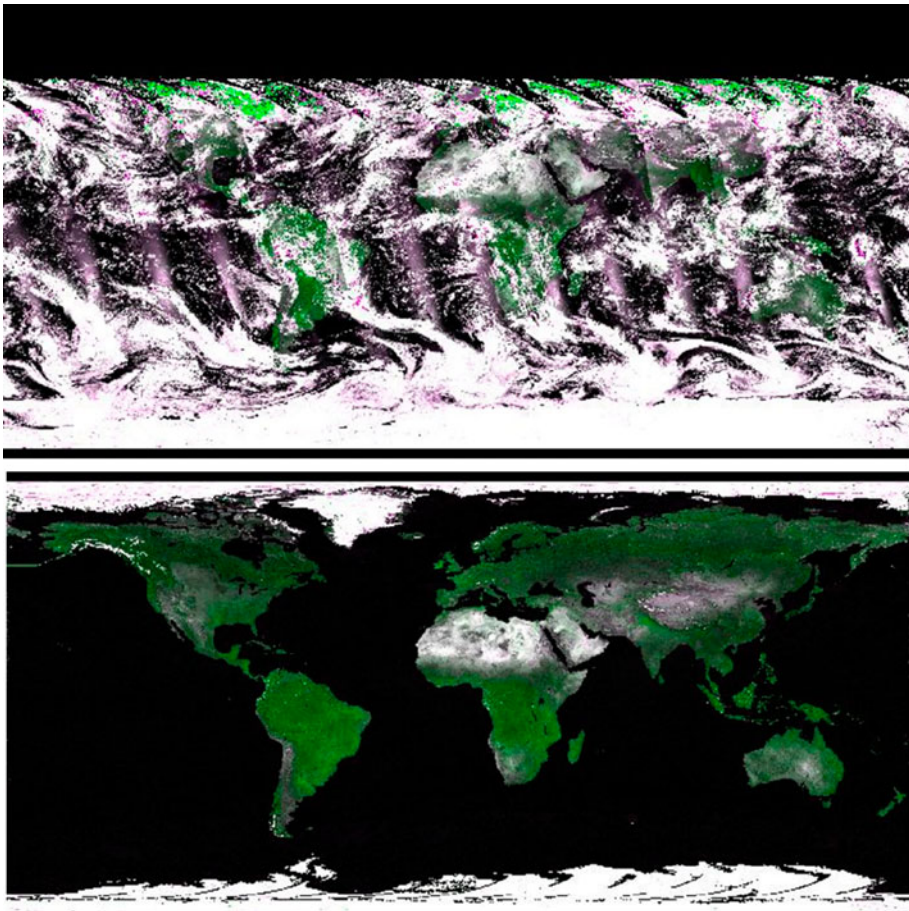

Figure 3. Original AVHRR data from the NASA 0.05° long-term AVHRR data-set on 7 January 2000 (top) and the reprocessed data (bottom). Color composite using bands 1 (blue), 2 (green), and 1 (red).

Table 2. Characteristics of the five GLASS products.

Product	Spatial resolution	Temporal resolution	Temporal range
Shortwave albedo	1–5 km, 0.05°	8-day	1981–2010
Incident solar radiation	5 km, 0.05°	3-h	2008–2010
Incident PAR	5 km, 0.05°	3-h	2008–2010
Longwave emissivity	1–5 km, 0.05°	8-day	1981–2010
LAI	1–5 km, 0.05°	8-day	1982–2012

validation results will be presented in the following sections. Table 2 summarizes the basic characteristics of these five GLASS products.

3. Shortwave broadband albedo product

3.1. Background

Land surface shortwave broadband albedo, representing the surface hemispheric reflectivity integrated over the solar spectrum (0.3–3.0 μm), is a fundamental component in determining surface radiation balance. Albedo has been identified by the Global Terrestrial Observing System (GTOS) as one of the essential climate variables (ECV).

The surface radiation budget is characterized by all-wave net radiation (R_n), which is the sum of the shortwave (S_n) and longwave (L_n) net radiation:

$$R_n = S_n + L_n = (1 - \alpha)S \downarrow + \varepsilon L \downarrow - \varepsilon \sigma T_s^4 \qquad (1)$$

where α is the surface shortwave albedo, $S\downarrow$ the incident shortwave radiation (Section 4), $L\downarrow$ the downward longwave radiation, σ the Stefan–Boltzmann constant, ε the surface thermal broadband emissivity (Section 6), and T_s the surface skin temperature.

Land surface albedo is highly variable both spatially and temporally. Variations in surface conditions, such as snow cover, vegetation phenology, and soil moisture, are all accompanied by significant changes in land albedo. Drought or forest fires can also lead to changes in surface albedo (Govaerts and Lattanzio 2008; Lyons, Jin, and Randerson 2008). In addition, humans can greatly change surface albedo through a variety of activities, such as deforestation (Loarie et al. 2011), irrigation (Zhu et al. 2011), and urbanization (Offerle et al. 2005). The recession of snow cover associated with warm periods in the Earth's history has led to greater absorption of solar energy (and hence amplified warming). Aerosols such as dust and soot may also greatly contaminate snow and reduce its albedo (Hansen and Nazarenko 2004; Xu et al. 2009).

Land surface albedo changes can be translated into equivalent carbon emissions through a calculation of radiative forcing (Betts 2000). Betts (2000) compared the radiative forcing associated with changes in surface albedo and atmospheric CO_2 and suggested that the positive forcing brought about by forestation-related decreases in albedo in temperate and boreal forest regions could offset the negative forcing expected from carbon sequestration. Deliberate land-use management (afforestation or reforestation) has been proposed and implemented as a mechanism to remove CO_2 from the atmosphere and sequester carbon in trees and soils. Davin and

de Noblet-Ducoudré (2010) showed that surface albedo increases as a result of deforestation (i.e. large-scale replacement of forests by grassland) has a cooling effect equivalent to -1.36 K globally. This effect is greater at high latitudes and impacts both land and ocean areas (Bala et al. 2007; Bonan 2008; Davin and de Noblet-Ducoudré 2010). At high latitudes, terrestrial changes in summer albedo have contributed substantially to recent warming trends. While the lengthening of the snow-free season increases local atmospheric heating by around 3 W m^{-2}, shrub and tree expansion resulting from climate warming is expected to amplify the land surface albedo feedback by two to seven times (Chapin et al. 2005).

Land surface albedo modulates the amount of solar radiation absorbed by surfaces and directly controls the distribution of solar radiation between the surface and the atmosphere, therefore significantly impacting climate and weather. Dethloff et al. (2006) found that the altered Arctic sea-ice and snow albedo can trigger changes in the Arctic and North Atlantic Oscillation pattern with serious implications for European climate. Chapin et al. (2005) synthesized field data from Arctic Alaska, showing that terrestrial changes in summer albedo contribute substantially to recent high-latitude warming trends. Data from the Boreal Ecosystem-Atmosphere Study (BOREAS) found that the winter albedos of the forest sites were significantly different from those used in the European numerical weather prediction models, leading to a systematic underestimation of the near-surface air temperature (Sellers et al. 1997).

Liang et al. (2010) showed that land surface albedo calculated from current general circulation models (GCM) are significantly different. Accurate satellite albedo products are needed to calibrate and validate model simulations. Regional surface albedo with an absolute accuracy of 0.02–0.05 for snow-free and snow-covered land is required by climate, biogeochemical, hydrological, and weather forecast models at a range of spatial (from a few hundred meters to 5–30 km) and temporal (from daily to monthly) scales (Dickinson 1983). To monitor the effects of the anticipated changes in land albedo on the global mean radiation budget, decade-scale trends in continental-mean surface albedo should be measured to an accuracy of 0.01 (Zhang et al. 2010).

Table 3 lists the existing global land albedo products. In addition to the need for an improvement in accuracy, it is necessary for the temporal range to be longer. The GLASS albedo product has the longest data record among the existing products.

Table 3. Summary of the current global shortwave broadband albedo products.

Albedo products	Spatial resolution	Temporal resolution (day)	Temporal range
MODIS	0.5 km, 1 km, 0.05°	8–16	2010–present
GlobAlbedo	0.05°	16	1998–2011
POLDER	1/12°	10	1996.11–1997.06, 2003.04–2003.10, 2005.07–2010.08
VEGETATION (Geoland2)	0.5°	10/30	1999–present
GLASS	1–5 km, 0.05°	8	1981–2010

3.2. GLASS albedo product

Most satellite albedo estimation algorithms consist of three steps (Liang et al. 2010): atmospheric correction, surface directional reflectance modeling, and narrowband to broadband conversion. However, the errors from each step may accumulate and affect the final accuracy of the albedo product. An alternative approach, the so-called 'direct estimation algorithm' estimates the surface albedo directly from top-of-atmosphere (TOA) observations, combining all procedures into one step through regression analysis and aiming only to give a best-estimate broadband albedo. In an earlier study, Liang, Strahler, and Walthall (1999) developed such a direct retrieval algorithm using a feed-forward neural network. It was later improved using linear regression analysis in each angular bin and was applied to MODIS data (Liang 2003), and also improved to produce very accurate daily snow/ice albedo more efficiently with a mean bias of less than 0.02 and a residual standard error of 0.04 (Liang, Stroeve, and Box 2005). This algorithm has been adopted for operationally mapping the land surface broadband albedo from the Visible/Infrared Imager/Radiometer Suite (VIIRS) in the NPP program and the future Joint Polar Satellite System (JPSS) program.

If a surface reflectance product (after atmospheric correction of the TOA observations) is available, the last two steps can be combined to convert the directional reflectance to broadband albedo. Cui, Mitomi, and Takamura (2009) developed such an empirical formula based on POLDER/ADEOS-1 multi-angle imagery data.

The GLASS albedo product is produced from both AVHRR (1981–1999) and MODIS (2000–2010) data. The albedo product from MODIS data is based on two direct albedo estimation algorithms from surface reflectance (AB1), TOA radiance (AB2, Qu et al. 2013), and the Statistics-based Temporal Filtering (STF) fusion algorithm that integrates these two intermediate albedo products (Liu et al. 2012).

The AB1 algorithm establishes a linear regression equation between surface directional reflectance and shortwave broadband albedo, specifically the shortwave white-sky albedo and black-sky albedo corresponding to the solar angle at local noon. It divides the solar illumination-view geometry space into small grids, which are called 'angular bins,' and then derives regression coefficients for each angular bin. Thus, the anisotropy of the land surface is empirically corrected. The AB2 algorithm is similar to AB1 algorithm, but builds the linear regression equation between TOA directional reflectance and shortwave broadband albedo. The STF algorithm is a Bayesian theory based approach, which regards different intermediate products as samples of the 'true' surface albedo with an inversion error and time discrepancy. Therefore, the optimal estimation of the 'true' albedo aims to determine the location with the maximum posterior probability. Thus, information from two different intermediate products is merged, and noise is compressed. In the case of no valid sample in the temporal filtering window, a-priori distribution of albedo is adopted to fill the gap.

The albedo product from AVHRR data is based on a similar direct estimation (AB2) algorithm from the TOA observations (Liu et al. 2013).

Extensive validation activities have been conducted and some results have been reported by Liu et al. (2013). Directly comparing the results to ground measurements at the homogeneous FLUXNET sites, the GLASS albedo product shows reasonable consistency with the magnitude and trend of ground measurements, with a bias less

than 0.001 and root mean square error (RMSE) less than 0.05 on clear days. The cross comparison shows that GLASS albedo product has accuracy similar to that of the MODIS MCD43B3 product whose data is marked by 'good' quality flag. Another validation study (Hu et al. 2013) demonstrated that GLASS albedo captured the spatial patterns better than MODIS albedo in northern China, especially over cropland and grassland.

Since we were unable to find reliable ground measurements for validating land albedo from AVHRR data, consistency tests were executed. The results indicate that the retrieved long-term albedo record is very stable. Figure 4 shows examples of long-term albedo values from both AVHRR and MODIS data at some stable sites.
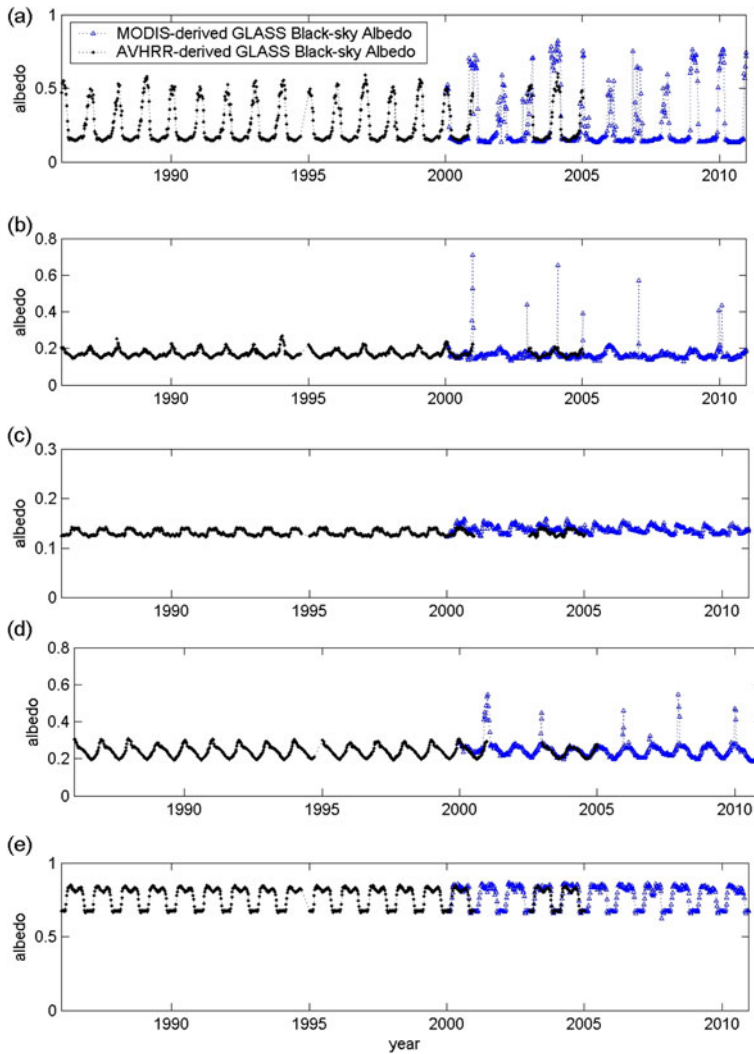

Figure 4. GLASS albedo product at five sites: (a) Fort_Pack, 48.3079N, −105.101E, glassland; (b) ARM_SGP_Main, 36.605N, −97.4884E, cropland; (c) Duke_forest_hardwoods, 35.9736E, −79.1004N, mixed forest; (d) Naiman_site, 42.9333E, 120.700N, desert; (e) NASA-SE, 66.4797E, −42.5002N, ice sheet.
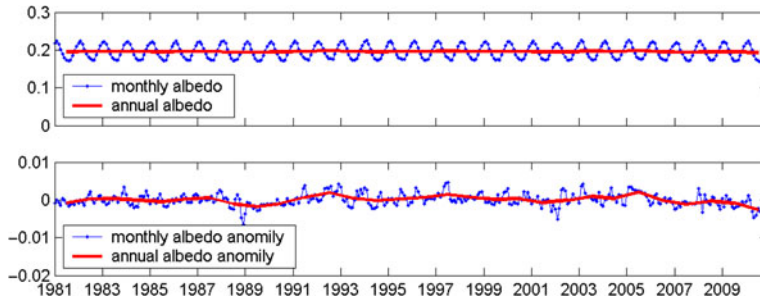
Figure 5. Global average albedo and anomalies on land surfaces.

   The average land surface albedo and its anomaly are shown in Figure 5. The average albedo over land surface is about 0.2 not including the Antarctic region. There are significant seasonal variations. Although there is no single identifiable overall trend, we can clearly identify a decreasing trend after 2005 and an increasing trend from the late 1980s and early 1990s. The detailed spatial and temporal variations of global albedo from GLASS albedo product are displayed in Figure 6. There are multiple factors resulting in the variations at different spatial and temporal scales. He et al. (2013) found from the GLASS albedo product that a large decrease in surface albedo over Greenland after 2000 (-0.0024 yr^{-1}) mainly occurred at
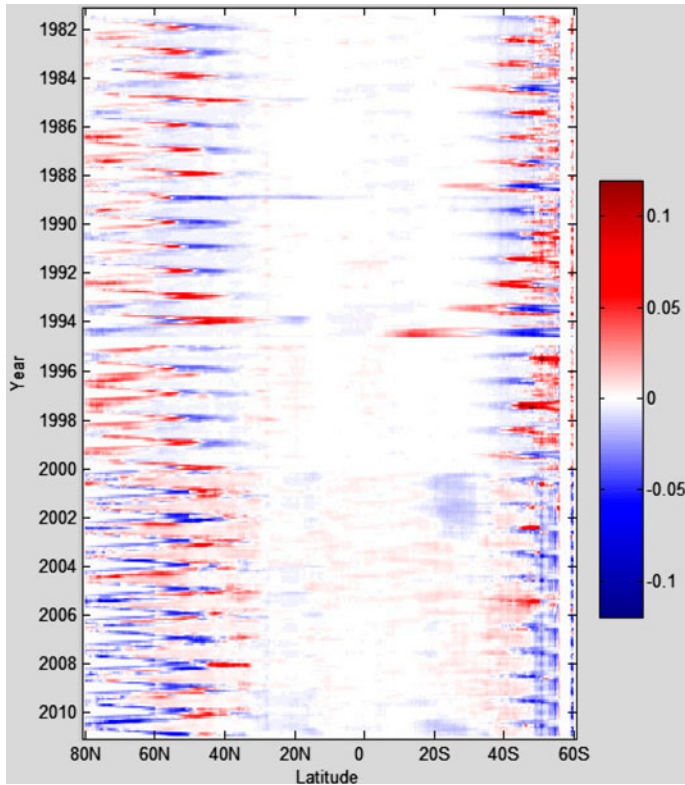

Figure 6. Spatial and temporal variations of global land surface albedo anomalies.

elevations 1000–1500 m above sea level (-0.0059 yr^{-1}) associated with surface temperature increase. Shi and Liang (2013) found that the albedo increase over Tibetan Plateau is highly correlated with the increase in snow cover. More studies are necessary to evaluate the causes of the variations in albedo.

4. Incident PAR product

4.1. Background

Incident PAR in the visible spectrum (400–700 nm) is a key variable in ecological modeling. Many ecosystem models calculate biomass accumulation as linearly proportional to incident PAR. Information on the spatial and temporal distribution of PAR, representing a control on the evapotranspiration (ET) process, is required for modeling the hydrological cycle and for estimating global oceanic and terrestrial net primary productivity (NPP).

Radiation, temperature, and water interact to impose complex and varying limitations on vegetation activity in different parts of the world. Nemani et al. (2003) estimated that radiation limits vegetation growth over 27% of Earth's vegetated surface. Almost all ecosystem models contain the physiological processes involved in photosynthesis and stomatal regulation that control the exchange of water vapor and carbon dioxide between vegetation canopies and the atmosphere. Gross primary productivity (GPP) of the vegetation canopy is often calculated by production efficiency models with inputs consisting of remote sensing products at varied spatial scales:

$$GPP = \sigma \times fPAR \times PAR$$

where σ is the radiation efficiency factor, *fPAR* represents the fraction of the *PAR* absorbed by the green vegetation. *fPAR* has been produced as a satellite product from many sensors, but thus far PAR has not. Cramer et al. (1999) inter-compared models and found that many widely used models utilize the production efficiency principles, such as Carnegie-Ames-Stanford approach (CASA) (Potter et al. 1993), a simple biosphere model (SiB) (Sellers et al. 1986), and GLObal Production Efficiency Model (GLO-PEM) (Prince and Goward 1995). The MODIS PSN/NPP product algorithm (MOD17) is also based on this formulation (Zhao, Running, and Nemani 2006). All these models require inputs of PAR data.

Few land surface global PAR products exist, since most global radiative flux data-sets do not include PAR, so users historically converted incident shortwave radiation (insolation) to PAR using an empirical constant around 0.5. Several studies from ground measurements have indicated that this ratio is not a constant, however. Jacovides et al. (2003) found that this ratio varies from 0.460 to 0.501 for hourly measured values. Alados, Foyo-Moreno, and Aslados-Arboledas (1996) also documented seasonal and daily variations in the ratio. It is smaller and more variable in the winter season than in the summer season, and is usually low at noon. Recent studies have also confirmed the earlier findings (Wang et al. 2007; Xia et al. 2008).

The MODIS science team must currently disaggregate the coarse-resolution ($1.00° \times 1.25°$) reanalysis solar radiation product from the Data Assimilation Office (DAO) (now the Global Modeling and Assimilation Office) as forcing data to

produce the 1-km PSN/NPP product (MOD17) (Zhao, Running, and Nemani 2006). Since that data-set does not include PAR, the MOD17 algorithm simply calculates PAR as 45% of insolation. Many other studies have also found significant impacts of solar radiation on GPP/NPP calculations (Liu et al. 1997; Hicke 2005).

NASA has recently produced a high-resolution (9.3 km) 12-year (1997–2009) global daily PAR product over oceans from SeaWiFS and MODIS data (Frouin 2007), but currently there is no corresponding high-resolution global PAR product over land surfaces available. The GLASS PAR product fills this gap for a temporal range of at least three years.

4.2. GLASS PAR product

There are two broad types of algorithm used for estimating incident solar radiation from satellite observations (Liang et al. 2010). The first approach is to use retrieved cloud and atmospheric parameters from other sources, with measured TOA radiance/flux acting as a constraint. These parameters have been used for estimating insolation from the Clouds and the Earth's Radiant Energy System (CERES) (Wielicki et al. 1998), the International Satellite Cloud Climatology Project (ISCCP) (Zhang et al. 2004), Global Energy and Water Cycle Experiment (GEWEX) (Pinker et al. 2003), and the Spinning Enhanced Visible and Infrared Imager (SEVIRI) (Deneke, Feijt, and Roebeling 2008). This approach has a clear physical basis, but the use of multiple atmospheric and surface products means that these products have coarse spatial resolutions that are unable to meet the requirements of many land-based applications.

The second approach is to establish the relationship between the TOA radiance and surface incident insolation based on extensive radiative transfer simulations. This idea was first applied to analyze the Earth Radiation Budget Experiment (ERBE) data (Li and Leighton 1993; Li et al. 1993). Liang et al. (2006) and Liu et al. (2008) generated the PAR and insolation products from MODIS data directly based on the Look-up Table (LUT) method. A similar approach has been used for Geostationary Operational Environmental Satellites (GOES) (Zheng, Liang, and Wang 2008) and AVHRR (Liang et al. 2007b). The basic framework of the algorithms is presented by Liang et al. (2006) in the case of estimating incident PAR from MODIS data. The main approach of this algorithm is the use of multi-temporal signatures from MODIS data. The outputs include direct and diffuse PAR, insolation, and other intermediate variables. The algorithm was later extended to estimate PAR from AVHRR and GOES data. In the follow-up studies, a series of refinements and improvements have been made. For example, MODIS surface reflectance product (MOD09) was used to map PAR over China from MODIS data (Liu et al. 2008). This algorithm has been extended to estimate PAR from GOES data (Zheng, Liang, and Wang 2008) by taking into account topographic effects. The algorithm was also extended to estimate insolation over China from imagery of Geostationary Meteorological Satellite (GMS) 5 by considering water vapor and the surface elevation (Lu et al. 2010). Huang et al. (2011) further extended the LUT scheme to estimate insolation by combining the Multifunctional Transport Satellite (MTSAT) data and MODIS data products. As a result, the algorithm becomes highly robust for multiple geostationary and polar-orbiting satellite data, and the accuracy has steadily improved.
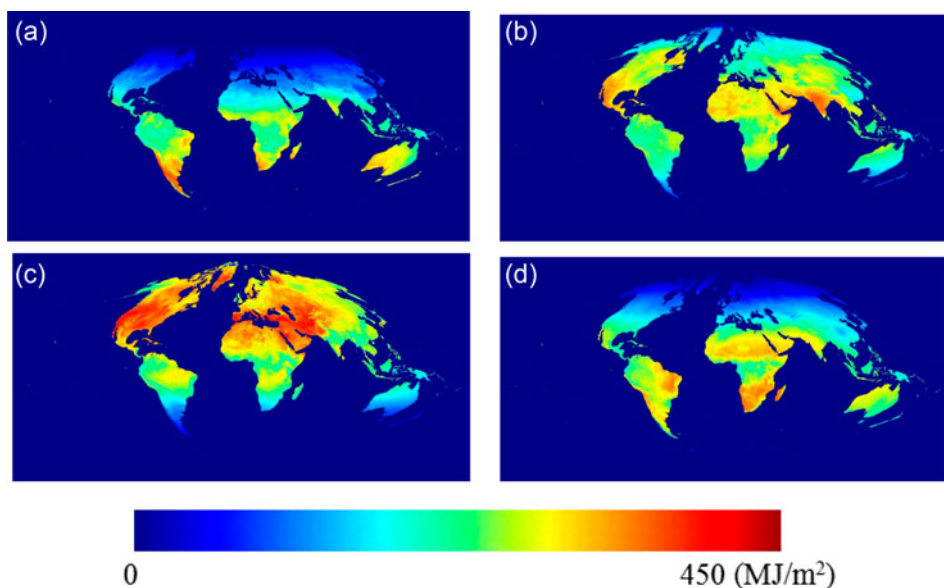
Figure 7. Global land surface monthly integrated incident PAR in 2008 at 5 km spatial resolution calculated from GLASS PAR product in (a) January, (b) April, (c) July, and (d) October.

The GLASS solar radiation products are based on four geostationary satellites (two GOES, MSG, and MTSAT) and MODIS data. Each geostationary satellite covers only one longitude zone in the low-latitude regions less than 60°. The polar-orbiting MODIS sensor collects daily data globally, but has gaps in low-latitude regions. Combinations of these data provide frequently refreshed global coverage. A detailed description of the algorithms for generating the GLASS solar radiation products is given by Zhang et al. (2013). The basic algorithms are based on the approach developed in previous studies with a series of refinements suitable for operational production. The major advance is the combination of procedures for integrating solar radiation products from multiple satellite data-sets. Figure 7 illustrates the monthly PAR calculated from the GLASS PAR product.

Zhang et al. (2013) validated the products using ground measurements at eight sites (two SURFRAD sites, three AERONET sites, one CarbonEuropeIP site, and two sites in China), the overall R^2, bias, and RMSE is 0.85, 14.3 W m^{-2}, and 47.5 W m^{-2}, respectively. More validation studies are under way.

5. Incident shortwave solar radiation product

Incident short radiation at land surfaces is needed to address a variety of scientific and application issues relating to climate trends, hydrologic, biophysical and biochemical modeling, solar energy applications, and agriculture (Liang et al. 2010; Wild 2012). Altering surface radiative forcing will lead to significant adjustments in surface temperature, moisture, and fluxes during the consequent complex land surface thermodynamic and hydrological processes. Thus, it can be expected to affect the surface heat and moisture budgets as well as biological

productivity. The observed reduction in land surface radiation during the past 30 years (1960–1990), the so-called 'dimming effect,' and the more recent evidence of a reversal in 'dimming' in some locations since 1990 will likely have several consequences on the climate and environment, notably on the hydrological cycle, cryosphere, Earth energy budget, and carbon cycle (Mercado et al. 2009; Wild 2012). However, the quality and spatial representativeness of the underlying surface observational data have been and continue to be under debate. Satellite products can address the spatial sampling issue, however, the temporal trends in the different satellite products are less consistent (Wild 2012), and the inversion algorithms require improvement.

Terrestrial ET uses on average approximately 59% (from 48% to 88% from different models) of the surface net energy (Trenberth, Fasullo, and Kiehl 2009), which is largely determined by surface incident solar radiation. In fact, many satellite ET estimation algorithms, including the MODIS ET product (MOD16), are directly dependent on incident solar radiation (Wang and Dickinson 2012). To initiate, calibrate, diagnose, and validate these algorithms and models, accurate inputs of solar radiation data-sets are a necessity. For example, the World Meteorological Organization (WMO) has specific requirements of spatial resolution and uncertainty for three applications (see Table 4).

The current global radiative flux data-sets derived mostly from satellite observations have much coarser spatial resolutions, such as the CERES product (Wielicki et al. 1998) at a spatial resolution of 140 km from 1997 to today, the ISCCP product on a 280 km equal-area global grid from 1983 to 2008 (Zhang et al. 2004), and the GEWEX surface radiation budget (SRB) product at a spatial resolution of $1° \times 1°$ from 1983 to 2007 (Pinker et al. 2003) (see Table 5).

Current insolation products used mostly for climate studies do not have the accuracy required for land-based applications. Gui et al. (2010) compared three

Table 4. WMO observation requirements for surface downward shortwave irradiance by Space program. NWP: Numerical Weather Prediction, AOPC: Atmospheric Observation Panel for Climate. (http://www.wmo-sat.info/db/variables/view/50, updated on 23 June 2011).

	Uncertainty goal (W m^{-2})	Uncertainty threshold (W m^{-2})	Horizontal resolution goal (km)	Horizontal resolution threshold (km)
Global NWP	1	20	10	100
Agricultural meteorology	N/A	N/A	1	20
Climate-AOPC	5	10	25	100

Table 5. Summary of the current global incident shortwave radiation satellite products.

Insolation products	Spatial resolution	Temporal resolution	Temporal range
ISCCP	280 km	3-h	1983–2008
GEWEX-SRB	1°	3-h	1983–2007
CERES	140 km	3-h	1997–present
GLASS	5 km	3-h	2008–2010

satellite-based surface insolation data-sets (GEWEX-SRB, ISCCP-FD, and CERES-FSW) and demonstrated large biases in Southeast Asia, the Tibet Plateau, and Greenland. Hicke (2005) found that global mean solar radiation from the National Center for Environment Prediction (NCEP) exceeded that from ISCCP by 16%, and locally, relative differences amounted to up to 40% in the mean and 10% in the trend of solar radiation, and varied positively and negatively across the globe. Xia et al. (2006) found that the NCEP reanalysis solar radiation data exceeded surface observations by 40 to more than 100 W m^{-2}.

The MODIS science team must currently disaggregate the coarse-resolution (1.00° × 1.25°) Data Assimilation Office (DAO) (now the Global Modeling and Assimilation Office) reanalysis solar radiation product to provide the forcing data to produce the 1-km ET product from MODIS data (MOD16) (Mu et al. 2007; Mu, Zhao, and Running 2011). Berg et al. (2005) pointed out that a bias on many of the reanalysis fields limits their use for hydrological modeling. Liu, Chen, and Cihlar (2003) bilinearly interpolated NCEP reanalysis data of around 0.9° into 1km to calculate daily ET at 1km resolution over the entire Canadian landmass in 1996 using the boreal ecosystem productivity simulator (BEPS). They found the daily total radiation in the NCEP data-set was 20–40% higher than the weather station measurements and had to correct this overestimation with a reduction coefficient for each month, determined by data from all 96 Canadian stations. In the NASA ET ESDR White Paper, Wood and Kimball (2007) stated that the desired spatial resolution of incident solar radiation product is 5 km.

The following user communities may have use for the insolation product (Liang et al. 2007a): (1) Hydrologists/ecologists for characterizing surface fluxes, and managing water and carbon resources; (2) Agronomists for monitoring crops, estimating water requirements, and predicting yields at farm to continental scales; (3) Federal agency officials involved in water resource allocation, crop yield assessment, and drought monitoring; (4) Urban and regional planners for mitigating heat island effects; and (5) Power plant administrators for estimating available solar energy.

For the insolation estimation from GMS-5 data (Lu et al. 2010), the RMSE and bias of hourly estimates is 76.6 W m^{-2} and 8 W m^{-2}, respectively. The daily estimates have an average RMSE of 29.16 W m^{-2} (17.7%) under all-sky conditions, which is relatively comparable to the results of other studies on using GMS-5 (Tanahashi et al. 2001; Kawai and Kawamura 2005). The RMSE of instantaneous and hourly insolation estimates from MTSAT is 97.4 W m^{-2} and 89.0 W m^{-2}, respectively (Huang et al. 2011). For comparison, Gui et al. (2010) assessed GEWEX, ISCCP-FD, and CERES-FSW data-sets with ground measurements collected at 36 globally distributed sites from 2000 to 2002 and reported an RMSE of 101.7–123.2 W m^{-2}.

The GLASS insolation algorithm is almost identical to that discussed in Section 4.2 with a few differences, and the preliminary validation results are very encouraging. Zhang et al. (2013) validated the instantaneous insolation product using ground measurements at eight sites (two SURFRAD sites, three AERONET sites, one CarbonEuropeIP site, and two sites in China), the overall R^2, bias, and RMSE is 0.87, 7.5 W m^{-2}, and 103.6 W m^{-2}, respectively. Huang et al. (2013) validated the instantaneous GLASS insolation product using ground measurements at 22 sites in the arid and semi-arid regions of China and found the R^2 at every site except one is larger than 0.8, and RMSE ranges from around 90 to 130 W m^{-2}.

S. Liang et al.

Table 6. Comparison of retrieved 3 h GLASS insolation product, the International Satellite Cloud Climatology Project—Flux Data (ISCCP-FD), CERES model B, and the CALISPO, CERES, Cloudsat and MODIS (CCCM) enhanced product in 2008.

| | | | | | | | CERES | | | | | |
| | Retrieved DSSR | | | ISCCP-FD | | | Model B | | | CCCM enhanced | | |
Site	R^2	Bias	RMSE	R^2	Bias	RMSE	R^2	Bias	RMSE	R^2	Bias	RMSE
Bondville	0.87	14.68	104.97	0.71	−7.06	149.88	0.84	12.9	119.5	0.82	−0.5	126.16
FortPeck	0.84	10.51	102.75	0.69	9.61	150.37	0.81	5.3	112.40	0.80	2.3	115.02
Goodwin Creek	0.91	−6.29	99.54	0.64	12.61	184.11	0.69	14.3	172.0	0.66	−3.8	179.35
Penn State	0.85	18.17	109.3	0.7	5.92	152.88	0.87	6.9	107.0	0.86	−8.6	111.18
Sioux Falls	0.81	11.52	114.41	0.65	37.83	168.85	0.62	−11.4	167.4	0.58	−37.8	178.77
Boulder	0.81	−12.8	126.38	0.72	6.49	154.96	0.34	−12.0	249.3	0.47	−43.0	214.41
DesertRock	0.92	−52.4	112.94	0.87	−42.4	125.27	0.52	−24.2	198.0	0.49	−26.6	206.38

After aggregating the spatial resolutions of the GLASS insolation product to match those of ISCCP and CERES, the validation results are shown in Table 6. It is clear that GLASS product is more accurate than these two existing products for these validation sites.

6. Longwave broadband emissivity product

Surface broadband emissivity ε is a key variable for estimating surface longwave net radiation, and an important parameter in climate, weather, and hydrological models. For dense vegetation and water surfaces, ε equals almost one. For non-vegetated surfaces, ε is much less than one. Unfortunately, due to the lack of reliable observations, a constant emissivity value or very simple parameterizations are adopted in land surface models and GCM. For example, the National Center for Atmospheric Research (NCAR) Community Land Model Version 2 (CLM2) calculates canopy emissivity from LAI and sets the soil and snow emissivities at 0.96 and 0.97, respectively (Bonan et al. 2002). A sensitivity study of the simulated energy balance to changes in emissivity over northern Africa and the Arabian Peninsula showed that, on average, a decrease of 0.1 in the soil emissivity increases the ground and air temperatures by approximately 1.1 and 0.8 °C, respectively, and decreases the net and upward longwave radiation by about 6.6 and 8.1 W m^{-2}, respectively (Zhou et al. 2003). Using offline CLM2 and coupled NCAR Community Atmosphere Models, CAM2–CLM2, Jin and Liang (2006) illustrated that the largest impacts on climate of surface emissivity occur over deserts, with changes up to 1–2 K in surface skin temperature, and 2-m surface air temperature, as well as evident changes in sensible and latent heat fluxes.

There is no broadband emissivity satellite product available, although several spectral emissivity products exist, as shown in Table 7. In theory, all spectral emissivity products can be converted into broadband emissivity using various conversion formulae, but creating a long-term broadband emissivity product from multiple satellite data is not an easy task since it requires a series of processing steps. The GLASS emissivity product is the only thermal-IR broadband emissivity ready for general use by the community. Note that it is a window broadband emissivity (8–13.5 μm) because it is found from extensive simulations from which it can calculate the longwave (2.5–200 μm) net radiation most accurately (Cheng et al. 2012).

The GLASS longwave emissivity product is generated from both AVHRR visible and near-infrared reflectance from 1981 to 1999 and MODIS seven black-sky albedos ranging from 2000 to 2010. GLASS emissivity algorithms (Cheng and Liang 2013b; Ren et al. 2013) classify the land surface into five types: water, snow/ice, bare soils, vegetated areas, and transition zones. The first two surface types are derived from the preprocessing steps and their emissivity values are set at 0.985 based on the ASTER spectral library (http://spclib.jpl.nasa.gov) and the MODIS UCSB spectral library (http://www.icess.ucsb.edu/modis/EMIS/html/em.html). The last three types are determined by the Normalized Difference Vegetation Index (NDVI) threshold values. GLASS broadband emissivity values are linearly related to shortwave spectral albedos and NDVI.

The method for estimating emissivity from AVHRR visible and near-infrared reflectance data (Cheng and Liang 2013a) is similar to that used for MODIS optical data. The major differences are that (1) the threshold values for identifying different

Table 7. Summary of the current global spectral emissivity products. IASI: Infrared Atmospheric Sounder Interferometer.

Products	Spatial and temporal resolutions, and temporal range	Wavelengths
CERES emissivity map (Wilber, Kratz, and Gupta 1999)	Global coverage, $10' \times 10'$, no temporal variation	12 spectral bands and one broadband (5–100 μm)
MODIS-based baseline fit database (Seemann et al. 2008)	Global coverage, 0.05°, monthly, 2003–2011	10 wavelengths (3.6–14.3 μm)
AIRS (Pequignot, Chedin, and Scott 2008)	30°N–30°S, monthly, April 2003–March 2006	3.7–14 μm (0.05 μm spectral resolution)
IASI (Capelle et al. 2012)	30°N–30°S, monthly, April 2007–March 2011	3.7–14 μm (0.05 μm spectral resolution)
ASTER (Gillespie et al. 1998)	Global discontinuous coverage, 90 m, 2000–present	5 bands
MODIS emissivity product (MOD11) (Wan and Li 1997)	Global coverage, 0.05°, 2000–present	6 bands (3.8–12.0 μm)
GLASS emissivity	Global coverage, 5 km (1981–1999) and 1 km (2000–2010)	1 broadband (8–13.5 μm)

land surface types differ, and (2) the input of the algorithm used for AVHRR is the reflectance of Channels 1 and 2, whereas the input data for the algorithm designed for MODIS is seven narrowband black-sky albedos.

The broadband emissivity derived from the MODIS albedos was validated by the field measurements conducted over desert areas in the USA and China; the absolute difference was found to be 0.02 (Cheng and Liang 2013b). The broadband emissivity derived from the AVHRR was consistent with that derived from MODIS data. The mean bias and RMSE of the difference between these two products was on the order of 0.001 and 0.01, respectively (Cheng and Liang 2013a).

In an independent validation study over desert areas (Dong et al. Forthcoming), the GLASS emissivity product is found to be in a very good agreement with field measurements. The range of the mean and standard deviation for all sand sample sites collected in the western region of Inner Mongolia Province is 0.0059 and 0.0114, respectively, and the difference between GLASS inversion emissivity and measured data is within ± 0.02. In the center of the Taklimakan desert, the average difference is less than 0.015. At the surface of the Dunhuang Gobi region, the average difference is 0.001 and 0.021 with different measurements, respectively. The combined mean emissivity difference between the GLASS product and the field measured results at all validation sites was about 1.1%.

Figure 8 displays the temporal variations of thermal broadband emissivity for a few major land cover types averaged from the global products. There are some minor disagreements in emissivity values from AVHRR and MODIS data, but in general the long-term values are stable and consistent. In comparison, the UW-Madison CIMSS emissivity values have much larger variations for most land cover types.
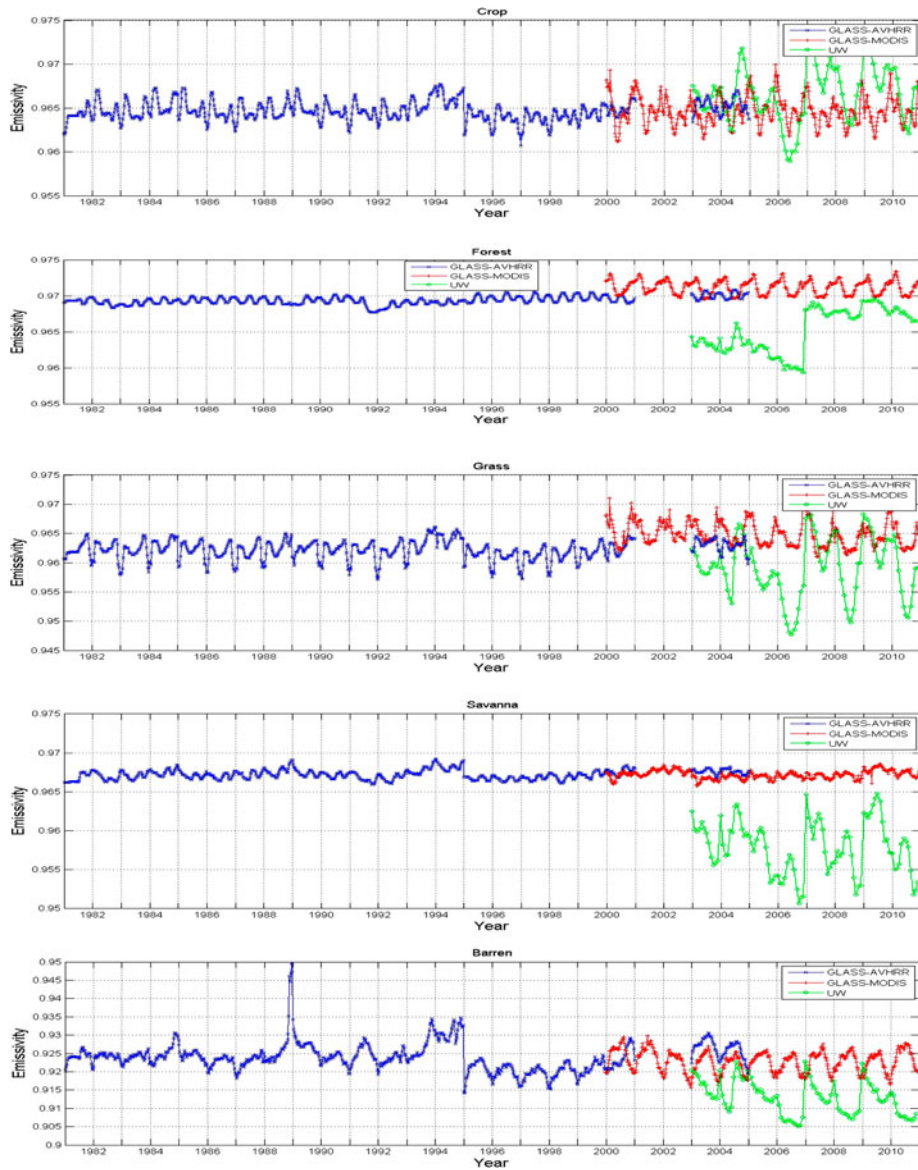
Figure 8. Long-term global surface thermal broadband emissivity mean values for five land cover types from the GLASS emissivity product. The UW-Madison CIMSS emissivity product (narrowband emissivity values are converted into the broadband emissivity using the published formula, Cheng et al. 2012) is also presented for comparison. Land cover maps are from the MODIS product: Majority_Land_Cover_Type_1 (MCD12C1 V5) and the land cover map from 2000 is used for the mean value calculation before 2000.

7. Leaf area index

7.1. Background

LAI, defined as one half of the total green leaf area per unit of horizontal ground surface area, is often called the *true LAI*. The true LAI multiplied by the clumping

index is termed the *effective LAI*. LAI measures the amount of leaf material in an ecosystem, which imposes important controls on processes, such as photosynthesis, respiration, and rain interception, which link vegetation to climate. Hence, LAI appears as a key variable in many models describing vegetation–atmosphere interactions, particularly with respect to the carbon and water cycles.

The models typically use satellite data based estimates of LAI in one of three ways: forcing for the model, validation of model output, and model assimilation. Buermann et al. (2001) reported using the NCAR Community Climate Model (CCM3) forced with AVHRR derived LAI that the use of satellite-derived fields leads to a notable warming and decreased precipitation over large parts of the northern hemisphere land area during the boreal summer. Such warming and drying result in reduced discrepancies between the simulated and observed near-surface temperature and precipitation fields.

The user community of the LAI includes at least the following three categories (Myneni et al. 2007): (1) Scientific: modelers of climate, primary production, ecology, hydrology, or crop production; (2) Public: meteorological organizations, deforestation, and desertification monitoring organizations, rapid response systems, pest risk evaluation companies, governments (for the implementation of international treaties such as the Kyoto protocol); and (3) Private: international agriculture and forestry companies, insurance companies, traders, amongst others. The WMO requirements for a LAI product are shown in Table 8.

Based on feedback from the user community in addition to the accumulated research experience, Myneni et al. (2007) proposed the following specifications for a global LAI product in the NASA ESDR White Paper (see Table 9):

- LAI accuracy of 0.5 LAI units to be achieved for corresponding global averages over individual biomes.
- Spatial resolution dependent on application: from 250 m (local ecological studies) to $0.25°$ (global climate studies).
- Temporal frequency from four days to monthly.
- Length of record starting from the beginning of AVHRR measurements (July 1981) and continuing into the future.

7.2. GLASS LAI algorithm and product validation

There are two methods for retrieving LAI from satellite data (Liang 2007): empirical methods and physical methods. The empirical methods are based on statistical relationships between LAI and spectral vegetation indexes, which are calibrated for distinct vegetation types using field measurements of LAI and reflectance data recorded by remote sensors or simulations from canopy radiation models. The physical methods are based on the inversion of canopy radiative transfer models through iterative minimization of a cost function, a LUT method, or various machine learning methods. Inversion techniques based on iterative minimization of a cost function require hundreds of runs of the canopy radiative transfer model for each pixel; they are therefore computationally too demanding. For operational applications, LUT and artificial neural networks (ANN) methods are two popular inversion techniques that are based on a pre-computed reflectance database. For

Table 8. WMO observation requirements for LAI by Space program. (http://www.wmo-sat.info/db/variables/view/98, updated on 3 June 2012).

Application area	Uncertainty goal (%)	Uncertainty threshold (%)	Spatial resolution goal (km)	Spatial resolution threshold (km)	Temporal resolution goal	Temporal resolution threshold (day)
Global NWP	5	20	2	50	24-h	10
High-resolution NWP	5	20	1	40	12-h	2
Hydrology	5	20	0.01	10	7-day	24
Agricultural meteorology	5	10	0.01	10	5-day	7
Climate-TOPC	5	10	0.25	10	24-h	30

Table 9. Summary of the current global LAI products; current products do not meet the user requirements. LAI products

	LAI type	Spatial resolution	Temporal resolution (day)	Temporal range
MODIS	True	1 km	8	2010–present
CYCLOPES	Effective	1/112°	10	1999–2003
GLOBECARBON	True	1/11.2°	10	1998–2007
Geoland2	True	1 km, 0.05°	10	1981–2012
GLASS	True	1–5 km, 0.05°	8	1981–2012

example, MODIS and MISR LAI products are based on the LUT method, and CYCLOPES LAI product is based on the ANN method.

The GLASS LAI algorithm (Xiao et al. 2013a, 2013b) is based on time-series reflectance data using general regression neural networks (GRNNs) trained by the fused LAI from MODIS and CYCLOPES LAI products and the reprocessed MODIS reflectance of the BELMANIP sites during the period 2001–2003. Two key unique features should be emphasized here. The first is to estimate the LAI annual profile by means of annual observations. Differing from the existing neural network methods that use only remote sensing data acquired at a specific time to retrieve LAI, GRNNs used for the GLASS LAI product use the surface reflectance of an entire year as the input. The output is therefore a one-year LAI for each pixel. The second feature is to train the ANNs by integrating both MODIS and CYCLOPE LAI products. Training with the representative samples is critical in any ANN algorithms. Instead of using simulation data, ANNs are trained with the fused time-series LAI from MODIS and CYCLOPES LAI products and the reprocessed MODIS reflectance.

The GLASS LAI product has been evaluated with both direct validation and inter-comparative studies (Xiao et al. 2013a, 2013b). By computing the RMSE and R^2 of each product over the LAI reference maps, it can be shown that the accuracy of
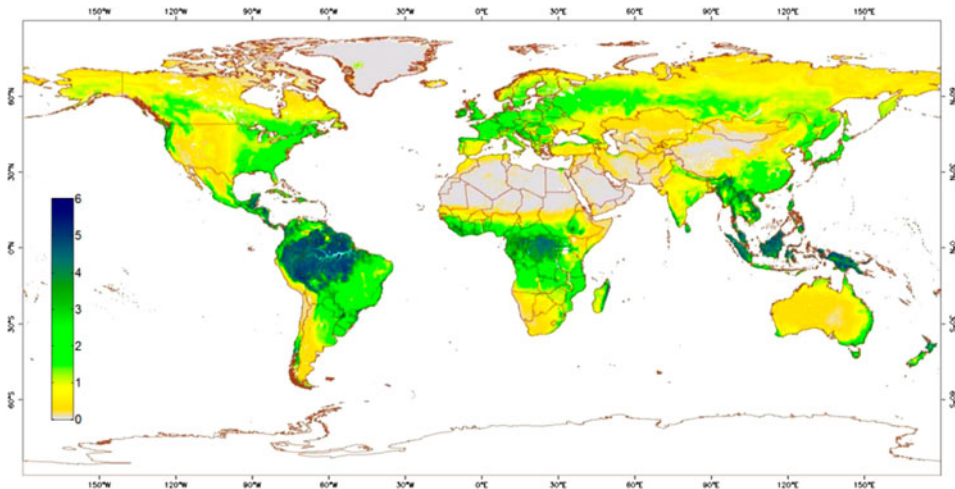
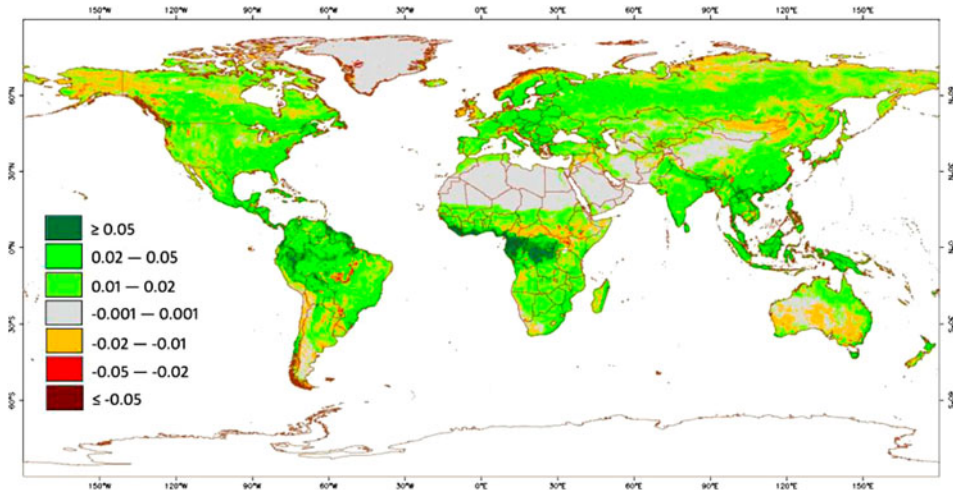Figure 9. Global average LAI for the period 1981–2012.

Figure 10. Slope of the linear fitting of global LAI changes from 1981 to 2012.

the GLASS LAI is clearly better than that of MODIS and CYCLOPES. Moreover, the GLASS LAI is more temporally continuous and spatially complete than the other tested products. The spatial patterns generated by GLASS are reasonable and consistent with good-quality MODIS and CYCLOPES LAI values. GLASS and CYCLOPES have smoother trajectories compared to the erratic fluctuations of the MODIS LAI. The GLASS LAI has more realistic and reasonable trajectories representing seasonal variations, especially for forested areas.

Extensive validation and comparison results have been shown in the previous works (Xiao et al. 2013a, 2013b). Fang et al. (2013) recently compared six major satellite LAI products, and the GLASS LAI product is reasonably consistent with other products.

The global annual average LAI distribution and anomalies are shown in Figures 9 and 10. Increased LAI can be found many parts of the world. It is interesting to note an overall increasing trend (Figure 11).
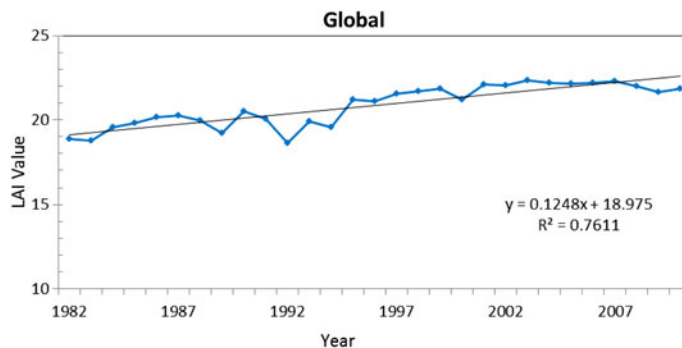
Figure 11. Temporal variations of global average LAI from 1981 to 2012 (*y*-axis has been multiplied by 10).

8. Brief summary

The high-resolution long-term GLASS data-set includes five products: albedo, emissivity, LAI, insolation, and PAR. The first three products span the period 1981–2012 (LAI) and 1981–2010 (albedo and emissivity) at 1–5 km and 8-day resolutions, and the last two products cover the period from 2008 to 2010, but have a high temporal resolution (3 h) and spatial resolution (5 km). The first three products are mainly based on AVHRR and MODIS data products, and the latter two radiation products use the five combined geostationary satellites and MODIS data.

When discussing each product, we began with a discussion of the potential applications and the limitations of the existing satellite products, resulting in the need for such an improved product. After reviewing the current inversion algorithms, we briefly outlined the GLASS product algorithms with an emphasis on their unique features, since most algorithms have been or will be published in peer-reviewed journals. Initial quality evaluation and validation analyses have been conducted. Their accuracy and inter-comparisons with the representative existing products have also been reported.

The evaluation and validation results have so far demonstrated that the GLASS products cover much longer temporal ranges, have high spatial and temporal resolutions, and achieve much higher accuracy compared to the existing products.

Efforts are currently under way to generate further products from the GLASS product production system with increasing reliance on the use of Chinese satellite data.

References

Alados, I., I. Foyo-Moreno, and L. Aslados-Arboledas. 1996. "Photosynthetically Active Radiation: Measurements and Modeling." *Agricultural and Forest Meteorology* 78 (1,2): 121–131. doi:10.1016/0168-1923(95)02245-7.

Bala, G., K. Caldeira, M. Wickett, T. J. Phillips, D. B. Lobell, C. Delire, and A. Mirin. 2007. "Combined Climate and Carbon-Cycle Effects of Large-scale Deforestation." *Proceedings of the National Academy of Sciences of the United States of America* 104 (16): 6550–6555. doi:10.1073/pnas.0608998104.

Berg, A. A., J. S. Famiglietti, M. Rodell, R. H. Reichle, U. Jambor, S. L. Holl, and P. R. Houser. 2005. "Development of a Hydrometeorological Forcing Data set for Global Soil

Moisture Estimation." *International Journal of Climatology* 25 (13): 1697–1714. doi:10.1002/joc.1203.

Betts, R. A. 2000. "Offset of the Potential Carbon Sink from Boreal Forestation by Decreases in Surface Albedo." *Nature* 408 (6809): 187–190. doi:10.1038/35041545.

Bonan, G. B. 2008. "Forests and Climate Change: Forcings, Feedbacks, and the Climate Benefits of Forests." *Science* 320 (5882): 1444–1449. doi:10.1126/science.1155121.

Bonan, G. B., K. W. Oleson, M. Vertenstein, S. Levis, X. Zeng, Y. Dai, R. E. Dickinson, and Z. L. Yang. 2002. "The Land Surface Climatology of the Community Land Model Coupled to the NCAR Community Climate Model." *Journal of Climate* 15 (22): 3123–3149. doi:10.1175/1520-0442.

Buermann, W., J. R. Dong, X. B. Zeng, R. B. Myneni, and R. E. Dickinson. 2001. "Evaluation of the Utility of Satellite-Based Vegetation Leaf Area Index Data for Climate Simulations." *Journal of Climate* 14 (17): 3536–3550. doi:10.1175/1520-0442.

Capelle, V., A. Chédin, E. Péquignot, P. Schlüssel, S. M. Newman, and N. A. Scott. 2012. "Infrared Continental Surface Emissivity Spectra and Skin Temperature Retrieved from IASI Observations over the Tropics." *Journal of Applied Meteorology and Climatology* 51 (6): 1164–1179. doi:10.1175/JAMC-D-11-0145.1.

Chapin, F. S., M. Sturm, M. C. Serreze, J. P. McFadden, J. R. Key, A. H. Lloyd, A. D. McGuire, et al. 2005. "Role of Land-Surface Changes in Arctic Summer Warming." *Science* 310 (5748): 657–660. doi:10.1126/science.1117368.

Cheng, J., and S. Liang. 2013a [Forthcoming]. "Estimating Global Land Surface Broadband Thermal Infrared Emissivity Using Advanced Very High Resolution Radiometer Optical Data." *International Journal of Digital Earth*. doi:10.1080/17538947.2013.783129.

Cheng, J., and S. Liang. 2013b. "A Novel Algorithm for Estimating Broadband Emissivity of Global Bare Soil using MODIS Albedo Product." *IEEE Transactions on Geoscience and Remote Sensing*, revised.

Cheng, J., S. Liang, Y. Yao, and X. Zhang. 2012. "Estimating the Optimal Broadband Emissivity Spectral Range for Calculating Surface Longwave Net Radiation." *IEEE Geoscience and Remote Sensing Letters* 10: 401–405. doi:10.1109/LGRS.2012.2206367.

Cramer, W., G. Churkina, B. Nemry, A. Ruimy, A. L. Schloss, D. W. Kicklighter, A. Bondeau, and I. B. Moore. 1999. "Comparing Global Models of Terrestrial Net Primary Productivity (NPP): Overview and Key Results." *Global Change Biology* 5: 1–15. doi:10.1046/j.1365-2486.1999.00009.x.

Cui, Y., Y. Mitomi, and T. Takamura. 2009. "An Empirical Anisotropy Correction Model for Estimating Land Surface Albedo for Radiation Budget Studies." *Remote Sensing of Environment* 113 (1): 24–39. doi:10.1016/j.rse.2008.08.007.

Davin, E. L., and N. de Noblet-Ducoudré. 2010. "Climatic Impact of Global-Scale Deforestation: Radiative Versus Nonradiative Processes." *Journal of Climate* 23 (1): 97–112. doi:10.1175/2009JCLI3102.1.

Deneke, H. M., A. J. Feijt, and R. A. Roebeling. 2008. "Estimating Surface Solar Irradiance from METEOSAT SEVIRI-Derived Cloud Properties." *Remote Sensing of Environment* 112 (6): 3131–3141. doi:10.1016/j.rse.2008.03.012.

Dethloff, K., A. Rinke, A. Benkel, M. Koltzow, E. Sokolova, S. K. Saha, D. Handorf, et al. 2006. "A Dynamical Link between the Arctic and the Global Climate System." *Geophysical Research Letters* 33. doi:10.1029/2005GL025245.

Dickinson, R. E. 1983. "Land Surface Processes and Climate-Surface Albedos and Energy Balance." *Advances in Geophysics* 25: 305–353. doi:10.1016/S0065-2687(08)60176-4.

Dong, L., J. Hu, S. Tang, and M. Min. Forthcoming. "Field Validation of GLASS Land Surface Broadband Emissivity Database Using Pseudo-Invariant Sand Dune Sites in Northern China." *International Journal of Digital Earth*.

Fang, H., C. Jiang, W. Li, S. Wei, F. Baret, J. Chen, J. Garcia-Haro, et al. 2013. "Characterization and Intercomparison of Global Moderate Resolution Leaf Area Index (LAI) Products: Analysis of Climatologies and Theoretical Uncertainties." *Journal of Geophysical Research – Biospheres*, submitted. doi:10.1002/jgrg.20051.

Frouin, R. 2007. *A Time Series of Photosynthetically Available Radiation at the Ocean Surface from SEAWIFS and MODIS Data*. (MEaSUREs funded proposal). Kyoto: Remote Sensing of the Marine Environment II.

Gillespie, A. R., S. Rokugawa, T. Matsunaga, J. Cothern, S. Hook, and A. Kahle. 1998. "A Temperature and Emissivity Separation Algorithm for Advanced Spaceborne Thermal Emission and Reflection Radiometer (ASTER) Images." *IEEE Transactions on Geoscience and Remote Sensing* 36 (4): 1113–1126. doi:10.1109/36.700995.

Govaerts, Y., and A. Lattanzio. 2008. "Estimation of Surface Albedo Increase During the Eighties Sahel Drought from Meteosat Observations." *Global and Planetary Change* 64 (3,4): 139–145. doi:10.1016/j.gloplacha.2008.04.004.

Gui, S., S. Liang, K. Wang, L. Li, and X. Zhang. 2010. "Assessment of Three Satellite-Estimated Land Surface Downward Shortwave Radiation Datasets." *IEEE Geoscience and Remote Sensing Letters* 7 (4): 776–780. doi:10.1109/LGRS.2010.2048196.

Hansen, J., and L. Nazarenko. 2004. "Soot Climate Forcing via Snow and ice Albedos." *Proceedings of the National Academy of Sciences of the United States of America* 101 (2): 423–428. doi:10.1073/pnas.2237157100.

He, T., S. Liang, Y. Yu, Q. Liu, and F. Gao. 2013. "Greenland Surface Albedo Changes 1981–2012 from Satellite Observations." *Geophysical Research Letters*, submitted.

Hicke, J. A. 2005. "NCEP and GISS Solar Radiation Data Sets Available for Ecosystem Modeling: Description, Differences, and Impacts on Net Primary Production." *Global Biogeochemical Cycles* 19: GB2006. doi:10.1029/2004GB002391.

Hu, Y., G. Jia, L. Bai, J. Hou, and H. Wang. 2013. "Comparison for Shortwave Albedo Products Based on Field Measurements from Coordinated Enhanced Observation System." *International Journal of Digital Earth*, submitted.

Huang, G., M. Ma, S. Liang, S. Liu, and X. Li. 2011. "A LUT-Based Approach to Estimate Surface Solar Irradiance by Combining MODIS and MTSAT Data." *Journal of Geophysical Research* 116 (D22): D22201. doi:10.1029/2011JD016120.

Huang, G., W. Wang, X. Zhang, S. Liang, S. Liu, T. Zhao, J. Feng, and Z. Ma. 2013. "Validation of GlASS-DSSR Products Using Surface Measurements Collected in Arid and Semi-Arid Region of China." *Journal of Mountain Science*, submitted.

Jacovides, C. P., F. S. Tymvios, D. N. Asimakopoulos, K. M. Theofilou, and S. Pashiardes. 2003. "Global Photosynthetically Active Radiation and its Relationship with Global Solar Radiation in the Eastern Mediterranean Basin." *Theoretical and Applied Climatology* 74 (3,4): 227–233. doi:10.1007/s00704-002-0685-5.

Jin, M., and S. Liang. 2006. "Improve Land Surface Emissivity Parameter for Land Surface Models Using Global Remote Sensing Observations." *Journal of Climate* 19 (12): 2867–2881. doi:10.1175/JCLI3720.1.

Kawai, Y., and H. Kawamura. 2005. "Validation and Improvement of Satellite-Derived Surface Solar Radiation over the Northwestern Pacific Ocean." *Journal of Oceanography* 61: 79–89. doi:10.1007/s10872-005-0021-7.

Li, Z., and H. G. Leighton. 1993. "Global Climatology of Solar Radiation Budgets at the Surface and in the Atmosphere from 5 Years of ERBE Data." *Journal of Geophysical Research* 98 (D3): 4919–4930. doi:10.1029/93JD00003.

Li, Z., H. G. Leighton, K. Masuda, and T. Takashima. 1993. "Estimation of SW Flux Absorbed at the Surface from TOA Reflected Flux." *Journal of Climate* 6 (2): 317–330. doi:10.1175/1520-0442.

Liang, S. 2003. "A Direct Algorithm for Estimating Land Surface Broadband Albedos from MODIS Imagery." *IEEE Transactions on Geoscience and Remote Sensing* 41 (1): 136–145. doi:10.1109/TGRS.2002.807751.

Liang, S., X. Li, and J. Wang, eds. 2012. *Advanced Remote Sensing: Terrestrial Information Extraction and Applications*. Oxford: Academic Press.

Liang, S., R. Pinker, S. Running, E. Wood, S. C. Tsay, and J. Townshend. 2007a. "PAR and Incident Solar Radiation, NASA ESDRs White Paper." http://landportal.gsfc.nasa.gov/Documents/ESDR/PAR-ISR_Liang_whitepaper.pdf.

Liang, S., A. Strahler, and C. Walthall. 1999. "Retrieval of Land Surface Albedo from Satellite Observations: A Simulation Study." *Journal of Applied Meteorology* 38 (6): 712–725. doi:10.1175/1520-0450.

Liang, S., K. Wang, X. Zhang, and M. Wild. 2010. "Review on Estimation of Land Surface Radiation and Energy Budgets from Ground Measurement, Remote Sensing and Model

Simulations." *IEEE Journal in Special Topics in Applied Earth Observations and Remote Sensing* 3 (3): 225–240. doi:10.1109/JSTARS.2010.2048556.

Liang, S., T. Zheng, R. Liu, H. Fang, S. C. Tsay, and S. Running. 2006. "Mapping Incident Photosynthetically Active Radiation (PAR) from MODIS Data." *Journal of Geophysical Research-Atmospheres* 111 (D15): D15208. doi:10.1029/2005JD006730.

Liang, S., T. Zheng, D. D. Wang, K. C. Wang, R. G. Liu, S. C. Tsay, S. Running, and J. Townshend. 2007b. "Mapping High-Resolution Incident Photosynthetically Active Radiation over Land from Polar-Orbiting and Geostationary Satellite Data." *Photogrammetric Engineering and Remote Sensing* 73: 1085–1089.

Liang, S. L. 2007. "Recent Developments in Estimating Land Surface Biogeophysical Variables from Optical Remote Sensing." *Progress in Physical Geography* 31 (5): 501–516. doi:10.1177/0309133307084626.

Liang, S. L., J. Stroeve, and J. E. Box. 2005. "Mapping Daily Snow/ice Shortwave Broadband Albedo from Moderate Resolution Imaging Spectroradiometer (MODIS): The Improved Direct Retrieval Algorithm and Validation with Greenland *in situ* Measurement." *Journal of Geophysical Research-Atmospheres* 110 (D10): D10109. doi:10.1029/2004JD005493.

Liu, J., J. M. Chen, and J. Cihlar. 2003. "Mapping Evapotranspiration Based on Remote Sensing: An Application to Canada's Landmass." *Water Resources Research* 39 (7). 1189. doi:10.1029/2002WR001680.

Liu, J., J. M. Chen, J. Cihlar, and W. M. Park. 1997. "A Process-Based Boreal Ecosystem Productivity Simulator Using Remote Sensing Inputs." *Remote Sensing of Environment* 62 (2): 158–175. doi:10.1016/S0034-4257(97)00089-8.

Liu, N., Q. Liu, L. Wang, S. Liang, J. Wen, Y. Qu, and S. Liu. 2012. "Mapping Spatially-Temporally Continuous Shortwave Albedo for Global Land Surface from MODIS Data." *Hydrology and Earth System Sciences Discussion* 9: 9043–9064. doi:10.5194/hessd-9-9043-2012.

Liu, Q., L. Wang, Y. Qu, N. Liu, S. Liu, H. Tang, and S. Liang. Forthcoming. "Preliminary Evaluation of the long-term GLASS Albedo Product." *International Journal of Digital Earth*. doi:10.1080/17538947.2013.804601.

Liu, R., S. Liang, H. He, J. Liu, and T. Zheng. 2008. "Mapping Photosynthetically Active Radiation from MODIS Data in China." *Remote Sensing of Environment* 112 (3): 998–1009. doi:10.1016/j.rse.2007.07.021.

Loarie, S. R., D. B. Lobell, G. P. Asner, Q. Mu, and C. B. Field. 2011. "Direct Impacts on Local Climate of Sugar-Cane Expansion in Brazil." *Nature Climate Change* 1 (2): 105–109. doi:10.1038/nclimate1067.

Lu, N., R. Liu, J. Liu, and S. Liang. 2010. "An Algorithm for Estimating Downward Shortwave Radiation from GMS-5 Visible Imagery and its Evaluation over China." *Journal of Geophysical Research-Atmospheres* 115 (D18): D18102. doi:10.1029/2009JD013457.

Lyons, E. A., Y. F. Jin, and J. T. Randerson. 2008. "Changes in Surface Albedo After Fire in Boreal Forest Ecosystems of Interior Alaska Assessed Using MODIS Satellite Observations." *Journal of Geophysical Research-Biogeosciences* 113: 15. doi:10.1029/2007JG000606.

Mercado, L. M., N. Bellouin, S. Sitch, O. Boucher, C. Huntingford, M. Wild, and P. M. Cox. 2009. "Impact of Changes in Diffuse Radiation on the Global Land Carbon Sink." *Nature* 458 (7241): 1014–1017. doi:10.1038/nature07949.

Mu, Q., F. A. Heinsch, M. Zhao, and S. W. Running. 2007. "Development of a Global Evapotranspiration Algorithm Based on MODIS and Global Meteorology Data." *Remote Sensing of Environment* 111: 519–536. doi:10.1016/j.rse.2007.04.015.

Mu, Q. Z., M. S. Zhao, and S. W. Running. 2011. "Evolution of Hydrological and Carbon Cycles under a Changing Climate. Part III: Global Change Impacts on Landscape Scale Evapotranspiration." *Hydrological Processes* 25 (26): 4093–4102. doi:10.1002/hyp.8367.

Myneni, R. B., R. R. Nemani, N. V. Shabanov, Y. Knyazikhin, J. T. Morisette, J. L. Privette, and S. W. Running. 2007. "LAI and FPAR." NASA Earth System Data Records (ESDR) White Papers. http://landportal.gsfc.nasa.gov/Documents/ESDR/LAI-FPAR_Myneni_whitepaper.pdf

Nemani, R., C. Keeling, H. Hashimoto, W. Jolly, S. Piper, C. Tucker, R. Myneni, and S. Running. 2003. "Climate-Driven Increases in Global Terrestrial Net Primary Production from 1982 to 1999." *Science* 330: 1560–1563. doi:10.1126/science.1082750.

Offerle, B., P. Jonsson, I. Eliasson, and C. S. B. Grimmond. 2005. "Urban Modification of the Surface Energy Balance in the West African Sahel: Ouagadougou, Burkina Faso." *Journal of Climate* 18 (19): 3983–3995. doi:10.1175/JCLI3520.1.

Pequignot, E., A. Chedin, and N. A. Scott. 2008. "Infrared Continental Surface Emissivity Spectra Retrieved from AIRS Hyperspectral Sensor." *Journal of Applied Meteorology and Climatology* 47: 1619–1633. doi:10.1175/2007JAMC1773.1.

Pinker, R. T., J. D. Tarpley, I. Laszlo, K. E. Mitchell, P. R. Houser, E. F. Wood, J. C. Schaake, et al. 2003. "Surface Radiation Budgets in Support of the GEWEX Continental-Scale International Project (GCIP) and the GEWEX Americas Prediction Project (GAPP), including the North American Land Data Assimilation System (NLDAS) Project." *Journal of Geophysical Research* 108: Art. No. 8844. doi:10.1029/2002JD003301.

Potter, C. S., J. T. Randerson, C. B. Field, P. A. Matson, P. M., Vitousek, H. A. Mooney, and S. A. Klooster. 1993. "Terrestrial Ecosystem Production: A Process Model Based on Global Satellite and Surface Data." *Global Biogeochemical Cycles* 7 (4): 811–841. doi:10.1029/93GB02725.

Prince, S. D., and S. N. Goward. 1995. "Global Primary Production: A Remote Sensing Approach." *Journal of Biogeography* 22: 815–835. doi:10.2307/2845983.

Qu, Y., Q. Liu, S. Liang, L. Wang, N. Liu, and S. Liu. 2013. "Improved Direct-Estimation Algorithm for Mapping Daily Land-Surface Broadband Albedo from MODIS Data." *IEEE Transactions on Geoscience and Remote Sensing*.

Ren, H., S. Liang, G. Yan, and J. Cheng. 2013. "Empirical Method to Map Global Broadband Emissivities over Vegetated Surfaces." *IEEE Transactions on Geoscience and Remote Sensing*.

Seemann, S., E. Borbas, R. Knuteson, E. Weisz, G. Stephenson, A. Huang, and J. Li. 2008. "A Global Infrared Surface Emissivity Database for Clear Sky Atmospheric Regression Retrievals." *Journal of Applied Meteorology* 47: 108–123. doi:10.1175/2007JAMC1590.1.

Sellers, P., F. Hall, R. Kelly, A. Black, D. Baldocchi, J. Berry, M. Ryan, et al. 1997. "BOREAS in 1997: Experiment Overview, Scientific Results, and Future Directions." *Journal of Geophysical Research* 102 (D24): 28731–28769. doi:10.1029/97JD03300.

Sellers, P. J., Y. Mintz, Y. C. Sud, and A. Dalcher. 1986. "A Simple Biosphere Model (SiB) for use within General Circulation Models." *Journal of the Atmospheric Sciences* 43 (6): 505–531. doi:10.1175/1520-0469.

Shi, Q., and Liang, S. 2013. "Characterizing the Surface Radiation Budget Over the Tibetan Plateau with Ground-Measured, Reanalysis, and Remote Sensing Datasets. Part 2: Spatio-Temporal Analysis." *Journal of Geophysical Research*, in revision.

Tanahashi, S., H. Kawamura, T. Matsuura, T. Takahashi, and H. Yusa. 2001. "A System to Distribute Satellite Incident Solar Radiation in Real-Time." *Remote Sensing of Environment* 75 (3): 412–422. doi:10.1016/S0034-4257(00)00183-8.

Tang, H., K. Yu, K. Jiang, X. Geng, and Y. Zhao. 2012. "A Time Series Method for Cloud Detection of Modis Surface Reflectance Images." *International Journal of Digital Earth*, submitted.

Trenberth, K. E., J. T. Fasullo, and J. Kiehl. 2009. "Earth's Global Energy Budget." *Bulletin of the American Meteorological Society* 90 (3): 311–323. doi:10.1175/2008BAMS2634.1.

Wan, Z., and Z. L. Li. 1997. "A Physics-Based Algorithm for Retrieving Land-Surface Emissivity and Temperature from EOS/MODIS Data." *IEEE Transactions on Geoscience and Remote Sensing* 35 (4): 980–996. doi:10.1109/36.602541.

Wang, K., and R. E. Dickinson. 2012. "A Review of Global Terrestrial Evapotranspiration: Observation, Modeling, Climatology, and Climatic Variability." *Reviews of Geophysics* 50: RG2005. doi:10.1029/2011RG000373.

Wang, Q., Y. Kakubari, M. Kubota, and J. Tenhunen. 2007. "Variation on PAR to global solar radiation ratio along altitude gradient in Naeba Mountain." *Theoretical and Applied Climatology* 87 (1–4): 239–253. doi:10.1007/s00704-005-0220-6.

Wielicki, B. A., B. R. Barkstrom, B. A. Baum, T. P. Charlock, R. N. Green, D. P. Kratz, R. B. Lee, et al. 1998. "Clouds and the Earth's Radiant Energy System (CERES): Algorithm Overview." *IEEE Transactions on Geoscience and Remote Sensing* 36 (4): 1127–1141. doi:10.1109/36.701020.

Wilber, A. C., D. P. Kratz, and S. K. Gupta. 1999. *Surface Emissivity Maps for Use in Satellite Retrievals of Longwave Radiation*, 35 pp. Hanover, MD: NASA.

Wild, M. 2012. "Enlightening Global Dimming and Brightening." *Bulletin of the American Meteorological Society* 93 (1): 27–37. doi:10.1175/BAMS-D-11-00074.1.

Wood, E., and J. S. Kimball. 2007. "White Paper on a Land Surface Evapotranspiration ESDR." NASA ESDR White Paper. http://landportal.gsfc.nasa.gov/Documents/ESDR/Surface_Hydrology_Wood_whitepaper.pdf

Xia, X., Z. Lib, P. Wang, M. Cribb, H. Chen, and Y. Zhao. 2008. "Analysis of Photosynthetic Photon Flux Density and its Parameterization in Northern China." *Agricultural and Forest Meteorology* 148 (6–7): 1101–1108. doi:10.1016/j.agrformet.2008.02.008.

Xia, X. A., P. C. Wang, H. B. Chen, and F. Liang. 2006. "Analysis of Downwelling Surface Solar Radiation in China from National Centers for Environmental Prediction Reanalysis, Satellite Estimates, and Surface Observations." *Journal of Geophysical Research-Atmospheres* 111: 9. doi:10.1029/2005JD006405.

Xiao, Z., S. Liang, J. Wang, P. Chen, and X. Yin. 2013a. "Leaf Area Index Retrieval from Multi-Sensor Remote Sensing Data Using General Regression Neural Networks." *IEEE Transactions on Geoscience and Remote Sensing*.

Xiao, Z., S. Liang, J. Wang, and X. Zhao. 2013b. "Long Time Series Global Land Surface Satellite (GLASS) Leaf Area Index Product Derived from MODIS and AVHRR Data." *Remote Sensing of Environment*, submitted.

Xu, B. Q., J. J. Cao, J. Hansen, T. D. Yao, D. R. Joswia, N. L. Wang, G. J. Wu, et al. 2009. "Black Soot and the Survival of Tibetan Glaciers." *Proceedings of the National Academy of Sciences of the United States of America* 106 (52): 22114–22118. doi:10.1073/pnas.0910444106.

Zhang, X., S. Liang, K. Wang, L. Li, and S. Gui. 2010. "Analysis of Global Land Surface Shortwave Broadband Albedo from Multiple Data Sources." *IEEE Journal in Special Topics in Applied Earth Observations and Remote Sensing* 3(3), 296–305. doi:10.1109/JSTARS.2010.2049342.

Zhang, X., S. Liang, G. Zhou, H. Wu, and X. Zhao. 2013. "Mapping Global Incident Downward Shortwave Radiation and Photosynthetically Active Radiation Over Land Surfaces Using Multiple Satellite Data." *Journal of Geophysical Research*, revised.

Zhang, Y. C., W. B. Rossow, A. A. Lacis, V. Oinas, and M. I. Mishchenko. 2004. "Calculation of Radiative Fluxes from the Surface to Top of Atmosphere Based on ISCCP and Other Global Data Sets: Refinements of the Radiative Transfer Model and the Input Data." *Journal of Geophysical Research-Atmospheres* 109 (D19): D19105. doi:10.1029/2003JD004457.

Zhao, M., S. Running, and R. Nemani. 2006. "Sensitivity of Moderate Resolution Imaging Spectroradiometer (MODIS) Terrestrial Primary Production to the Accuracy of Meteorological Reanalyses." *Journal of Geophysical Research* 111: G01002.

Zheng, T., S. Liang, and K. C. Wang. 2008. "Estimation of Incident PAR from GOES Imagery." *Journal of Applied Meteorology and Climatology* 47 (3): 853–868. doi:10.1175/2007JAMC1475.1.

Zhou, L., R. E. Dickinson, Y. Tian, M. Jin, K. Ogawa, H. Yu, and T. Schmugge. 2003. "A Sensitivity Study of Climate and Energy Balance Simulations with Use of Satellite-Derived Emissivity Data over Northern Africa and the Arabian Peninsula." *Journal of Geophysical Research* 108: 4795. doi:10.1029/2003JD004083.

Zhu, X. F., S. L. Liang, Y. Z. Pan, and X. T. Zhang. 2011. "Agricultural Irrigation Impacts on Land Surface Characteristics Detected From Satellite Data Products in Jilin Province, China." *IEEE Journal of Selected Topics in Applied Earth Observations and Remote Sensing* 4 (3): 721–729. doi:10.1109/JSTARS.2011.2106152.